GPS Solutions (2019) 23:118
https://doi.org/10.1007/s10291-019-0912-5

REVIEW ARTICLE

Estimation of snow depth using pseudorange and carrier phase observations of GNSS single-frequency signal

Yunwei Li[1] · Xin Chang[1] · Kegen Yu[2] · Shuyao Wang[1] · Jiancheng Li[1,3]

Received: 24 December 2018 / Accepted: 6 September 2019 / Published online: 17 September 2019

Abstract
A new method is proposed to estimate snow depth by using observations of the GNSS single-frequency signal collected by a ground-based receiver. The proposed method utilizes the pseudorange and carrier phase observations to form the geometry-free combination. Based on mathematical formulas of the amplitude attenuation factor, the pseudorange multipath error, and the carrier phase multipath error, a function is derived serving as the theoretical model that describes the relationship between the antenna height and the peak frequency of a series of function values associated with the range of satellite elevation angles. In the observation data processing stage, the moving average filtering method is used to remove the ionospheric delay from the combined observation series, followed by spectrum analysis to obtain the peak frequency, which is used to determine the antenna height and hence snow depth based on the theoretical model. A weighting method is proposed to combine individual snow depth estimates related to the use of signals of individual satellites to enhance the estimation accuracy. Each weighting coefficient is proportional to the maximum of the power spectral density of the combined observation series. The proposed method is substantiated by simulations and observations from geodetic-grade receivers, which can process multi-constellations and multi-frequency GNSS signals. Two field GNSS data sets collected in Heilongjing, China, and Colorado, USA, were used to evaluate the method. The results show that the root-mean-square error of GPS, BDS, and Galileo-based snow depth estimations is in the range of 2–6 cm when the topography around the GNSS receiver is flat.

Keywords Global navigation satellite system reflectometry (GNSS-R) · Snow depth estimation · GNSS single-frequency signal · Pseudorange and carrier phase combination

Introduction

Snow water equivalent (SWE), which is the product of snow depth and snow density, is an important parameter for water resource management and is an essential component within the earth's climate system (Tabibi et al. 2017; Henkel et al. 2018). Long-term changes in snow depth, SWE, and the extent of snow cover indicate climate changes (Barry 1996). Among the three snowfall measurements, only extent of snow cover can be easily measured using airborne or satellite remote sensing techniques (Estilow et al. 2015; Harpold et al. 2014).

Because of economic and other limiting factors, monitoring the distribution and variation of snow depth by using the traditional method with a high temporal and spatial resolution is infeasible. Although sonic measurement, snow pillows, and gamma radiation measurement have a higher temporal resolution of snow depth measurement (Sturm 2009; Garvelmann et al. 2013; Serreze et al. 1999), those methods have limited spatial coverage. The global navigation satellite system (GNSS) has been widely used for positioning, navigation, and timing. Except for these typical applications, GNSS has also been exploited for remote sensing, resulting in two new remote sensing techniques, GNSS radio occultation (GNSS-RO) and GNSS reflectometry (GNSS-R) (Yu et al. 2015). GNSS-R can be used to estimate the characteristics of the ocean and the land surface, such as ocean surface height, roughness, ground

✉ Kegen Yu
kegen.yu@foxmail.com

[1] School of Geodesy and Geomatics, Wuhan University, Wuhan 430079, China

[2] School of Environmental Science and Spatial Informatics, China University of Mining and Technology, 1 Daxue Road, Xuzhou 221116, Jiangsu, China

[3] Key Laboratory of Geophysical Geodesy, National Administration of Surveying, Mapping and Geoinformation, Wuhan 430079, China

vegetation condition, soil moisture, and snow depth (Small et al. 2010; Larson et al. 2008; Nievinski and Larson 2014a, b; Yu et al. 2014; Jin and Najibi 2014). A larger number of GNSS CORS (Continuously Operating Reference Station) have been established over the world, some of which are located in the cold regions and the recorded GNSS data can be exploited for snow depth estimation. Therefore, the GNSS-R-based snow depth estimation is cost-effective and can achieve high temporal and spatial resolution for snow depth estimation.

We proposed a snow depth estimation method using GNSS dual-frequency observations of pseudorange and carrier phase (Yu et al. 2018). Here, a combination method of GNSS single-frequency observations of pseudorange and carrier phase is proposed to estimate snow depth. The proposed method is more applicable in practice since almost all of the GNSS receivers could process single-frequency signals and record pseudorange and carrier phase observations. On the other hand, SNR (signal-to-noise ratio) observable is not always available, especially for early GNSS receivers and RINEX files. In addition, a range of receivers may not be able to record dual-frequency or triple-frequency signals. As a result, the existing SNR method, the dual-frequency and the triple-frequency phase combination method are not applicable in some cases.

In the next section, details of the proposed snow depth estimation method are presented. Then, the proposed method is tested comprehensively by using two field GNSS data sets which were collected by geodetic-grade multi-frequency receivers. Later, performance comparisons are also made with the SNR method under different GNSS constellations and signal frequencies using one of the two data sets. Finally, a summary is provided, and conclusions are drawn.

Proposed snow depth estimation method

This section presents the details of the proposed snow depth estimation method. The combination of pseudorange and carrier phase observations of GNSS single-frequency signal is studied, which is a function of the pseudorange multipath error and carrier phase multipath error. Then, modeling of the relationship between antenna height and peak frequency of the combined multipath error series, and weighting of individual satellite-based snow depth observations are described.

Combination of single-frequency pseudorange and carrier phase

The pseudorange and carrier phase observations ($\tilde{\rho}(t)$ and $\tilde{\varphi}(t)$) can be written as (Wellenhof et al. 2008),

$$\begin{aligned}\tilde{\rho}(t) &= d_{\mathrm{s,r}} + I + \Upsilon + \ell(t)\\ \lambda\tilde{\varphi}(t) &= \lambda(\tilde{\varphi}(t) + N) - \lambda N\\ &= d_{\mathrm{s,r}} - I + \Upsilon + \beta(t) - \lambda N\end{aligned} \tag{1}$$

where $d_{\mathrm{s,r}}$ is the Euclidian distance between the satellite and the receiver; I is the ionospheric delay; and Υ accounts for all other effects including clock errors and tropospheric delays; N is the integer ambiguity of carrier phase observations; $\ell(t)$ and $\beta(t)$ are the pseudorange multipath error and carrier phase multipath error in meters, which can be written as (Axelrad et al. 2005; Ozeki and Heki 2012):

$$\begin{aligned}\ell(t) &= \frac{2h\sin\theta(t)\cdot\alpha\cdot\cos\left(2\pi\frac{2h}{\lambda}\sin\theta(t)\right)}{1+\alpha\cos\left(2\pi\frac{2h}{\lambda}\sin\theta(t)\right)}\\ \beta(t) &= \frac{\lambda}{2\pi}\cdot\tan^{-1}\left(\frac{\alpha\sin\left(2\pi\frac{2h}{\lambda}\sin\theta(t)\right)}{1+\alpha\cos\left(2\pi\frac{2h}{\lambda}\sin\theta(t)\right)}\right)\end{aligned} \tag{2}$$

where h is the antenna height above the snow surface; $\theta(t)$ is the GNSS satellite elevation angle; λ is the GNSS signal wavelength; and α is the amplitude attenuation factor (AAF), which is related to the elevation angle, complex permittivity of snow and GNSS antenna gain (Nievinski and Larson 2014a, b).

The combination of pseudorange and carrier phase observations of single-frequency GNSS signals (code minus carrier phase, or CMC) is defined as (Blanco-Delgado and Haag 2011):

$$\mathrm{CMC}(t) = \tilde{\rho}(t) - \lambda\tilde{\varphi}(t) \tag{3}$$

Substituting (1) into (3), the Euclidean distance $d_{s,r}$ and Υ have been removed by the subtraction, yielding:

$$\mathrm{CMC}(t) = \ell(t) - \beta(t) + 2I(t) + \lambda N \tag{4}$$

Provided that the raw carrier phase observation does not have cycle slip or it is repaired, the last term related to integer ambiguity can be treated as a constant, so it does not affect the frequency and phase of the combined signal. Compared with the combined signal of pseudorange multipath error and carrier phase multipath error, the ionospheric delay has a much lower frequency and can be well recovered by low-pass filtering or ionospheric delay modeling and then removed by subtraction. By dropping those parameters, equation (4) becomes,

$$M(t) = \ell(t) - \beta(t) \tag{5}$$

That is, the combined raw pseudorange and carrier phase observation is equal to the combination of pseudorange multipath error and carrier phase multipath error.

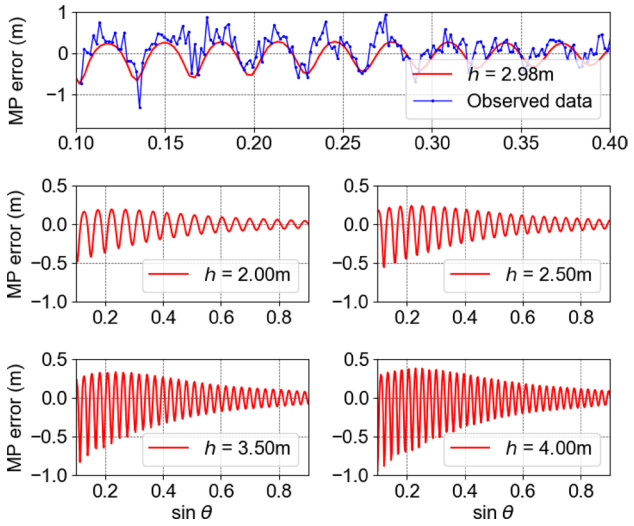

Fig. 1 Series of the combined multipath error calculated by (2) and (5) for GPS L1 signal

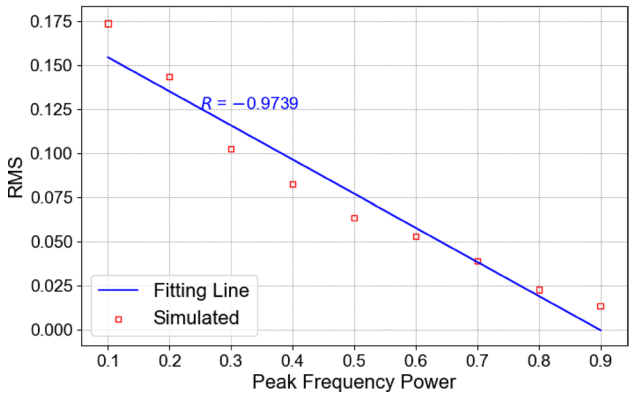

Fig. 2 RMS of the peak spectral frequency estimation error as a function of the power spectral density at the peak frequency

Figure 1 shows an example of the combined multipath error series with respect to sinθ calculated by (2) and (5), when the antenna height is 2.0 m, 2.5 m, 2.98 m, 3.50 m, and 4.0 m, respectively. The typical complex dielectric constant of dry snow surface (2.025–0.0005j) and the radiation pattern of GNSS antenna of TRM55971.00 are used to calculate the combined multipath error. It can be observed that there is a nearly constant oscillating period for the combined multipath error series with given antenna height. Due to the effect of the reflection coefficient of snow surface and antenna gain variation, the amplitude of the combined errors gradually attenuates with sinθ in general, although the attenuating rate can be different for different antenna heights. The combined multipath error series under different antenna heights exhibits significantly different oscillating patterns. Notice that a series which is the combination of real observations of pseudorange and carrier phase of GPS L1 signal is also shown in Fig. 1 (top panel), when the antenna height above the snow surface is 2.98 m. In addition, all of the simulation series shown in Fig. 1 have not taken the effect of ionospheric delay into account. The series of real observation combination shown in the top panel is the result after removal of ionospheric delay from the raw combination by the method introduced in the following section. Clearly, the results show good agreement between the values calculated by the theoretical formula given by (5) and the combination of the real pseudorange and carrier phase observations.

The oscillating period and peak frequency of the combined multipath error can be obtained by using Lomb–Scargle spectral analysis (Lomb 1976; Scargle 2003). The existence of measurement noise will significantly reduce the power spectral density at the peak frequency and slightly deviate the peak frequency from the noise-free one (Yu et al. 2018). In addition, the deviation is inversely proportional to the power spectral density at the peak frequency in general. Figure 2 shows an example of the RMS of the peak frequency estimation error as a function of the power spectral density at the peak frequency for GPS L1 band signal combination when the antenna height is 3.5 m. It can be observed that the RMS of the peak frequency estimation error significantly decreases with the increase in the power spectral density at the peak frequency. The correlation coefficient between the power spectral density at the peak frequency and the RMS of the peak spectral frequency estimation error is −0.9739, indicating a strong negative linear correction between them. This observation is helpful because it is possible to roughly estimate the accuracy of snow depth estimation of the proposed method based on the power spectral density at the peak frequency. Thus, in the presence of estimates from multiple satellites, an improved snow depth estimation accuracy can be obtained by weighting each snow depth estimate differently.

Conversion from peak frequency to snow depth

The height of a typical CORS antenna is assumed to range from 1.0 to 5.0 m, the radiation pattern of antenna TRM55971.00 is considered, and the snow permittivity is set to be 2.025–0.0005 j (Tiuri et al. 1984). Several different heights within the range of typical CORS antenna height are used to calculate the combined multipath error series theoretically by (2) and (5); the elevation angle series ranges from 5° to 30°. Notice that the ionospheric delays are not included in those simulated multipath error series. Then, the Lomb–Scargle spectrum analysis is carried out over the sequence of the combined errors under a specific antenna height to obtain the peak frequency. Repeating the procedure for all the selected antenna heights produces a sequence of peak frequencies. A suitable model free of contributions from ionospheric delays can be developed based on the

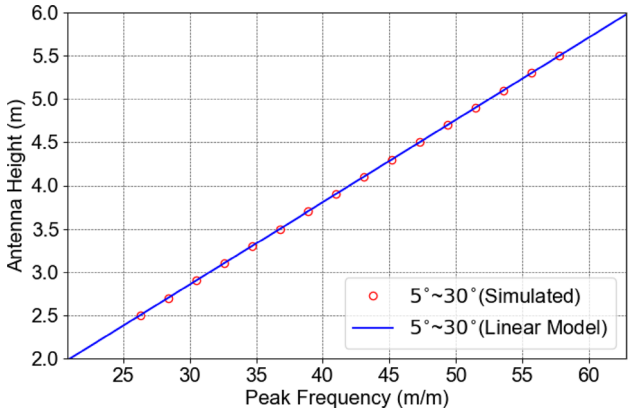

Fig. 3 Linear relationship between antenna height and peak frequency

Table 1 Fitting parameters for GPS, BDS, and Galileo

Satellite constellations	GNSS signal band	*a* (m)	*b* (m)	RMS (mm)
GPS	L1	0.0951	0.0016	0.5
	L2	0.1221	0.0026	0.7
BDS	B1	0.0960	0.0005	0.3
	B2	0.1241	0.0031	0.7
Galileo	E1	0.0951	0.0016	0.5
	E5	0.1257	0.0037	0.9

distribution pattern of the antenna height versus the peak frequency. Figure 3 shows an example of the antenna height with respect to the peak frequency for the combination of GPS L1 band multipath errors. It can be observed that the relationship between antenna height and peak frequency can be well described by a linear function. The least-squares fitting was used to establish the linear function, and the function for each satellite with a given GNSS signal frequency can be written as,

$$h_i = a \times f_i + b \tag{6}$$

where f_i is the peak frequency of the combined multipath series associated with the satellite of interest; a and b are the fitting parameters. Table 1 shows the fitting parameters for different GNSS signal frequency and fitting errors. Note that, although those models were developed based on a special antenna gain pattern (TRM55971.00) and reflection surface (dry snow), the antenna gain pattern and properties of reflection surface of snow (i.e., complex dielectric constant of snow) have marginal effect on the peak frequency of the combined multipath error series, as shown in Table 2. The fitting parameters of the linear model for GPS L1 band signal are very similar under two significantly different antenna gain patterns and snow surface dielectric constants (dry snow and wet snow). The error of antenna height estimations

Table 2 Fitting parameters for GPS L1 band signal with different complex dielectric constants of snow surface and antenna gain pattern

Antenna type	Complex dielectric constant of snow surface	*a* (m)	*b* (m)	RMS (mm)
TRM41249.00	2.025–0.0005j	0.0951	0.0016	0.5
	9.50–1.80j	0.0951	0.0018	0.3
TRM55971.00	2.025–0.0005j	0.0951	0.0015	0.8
	9.50–1.80j	0.0951	0.0016	0.5

caused by the difference in antenna gain pattern and dielectric constant is smaller than 1 mm.

As shown in Fig. 2, the RMS of the peak frequency estimation error is inversely proportional to the power spectral density at the peak frequency. Accordingly, the accuracy of GNSS-based antenna height and hence snow depth estimations is proportional to the power spectral density at the peak frequency. Thus, in the presence of observations relate to multiple satellites, an improved snow depth estimate can be obtained as the weighted sum of the individual estimates:

$$\Delta h = H - \frac{1}{\sum_{i=1}^{n} p_i} \cdot \sum_{i=1}^{n} \left(p_i h_i\right) \tag{7}$$

where p_i is the power spectral density at the peak frequency which is obtained by the combined multipath error series of the individual satellite; H is the antenna height when the ground is snow-free. The observation periods of the satellite signals are not required to be exactly the same, but the snow depth variation over space and observation duration should be negligible. Otherwise, the estimated snow depth would be the mean snow depth over the space and duration.

Removal of ionospheric delay

The terms introduced in (4) have different bands in the frequency domain. The frequency of the ionospheric delays is lower than 0.1 MHz, whereas the spectrum of combined multipath error is significant in the range of 1 MHz to several tens of MHz (Pugliano et al. 2016). This means that the ionospheric delays could be estimated by using the moving average method, which is a simple low-pass filter. For the combined raw observations with k samples from sample $t-k+1$ to sample t, the ionospheric delay can be estimated by:

$$\widetilde{2I}(t) = \frac{\sum_{i=t-k+1}^{t} \widetilde{\mathrm{CMC}}(i)}{k} \quad \text{with} \quad t \geq k \tag{8}$$

Then, the estimated ionospheric delays are removed from the raw combinations by:

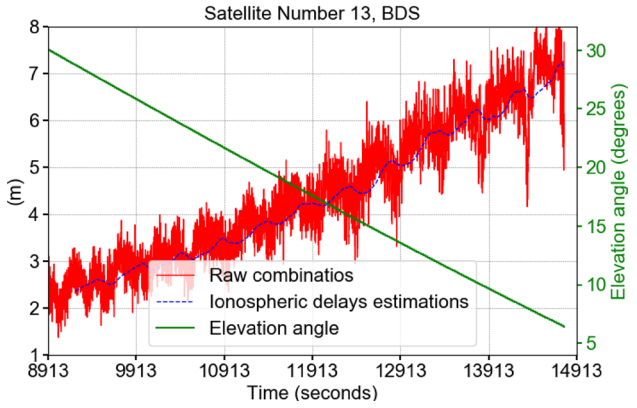

Fig. 4 Example of the time series of raw combinations of CMC for BDS B1 band signal and ionospheric delays estimations

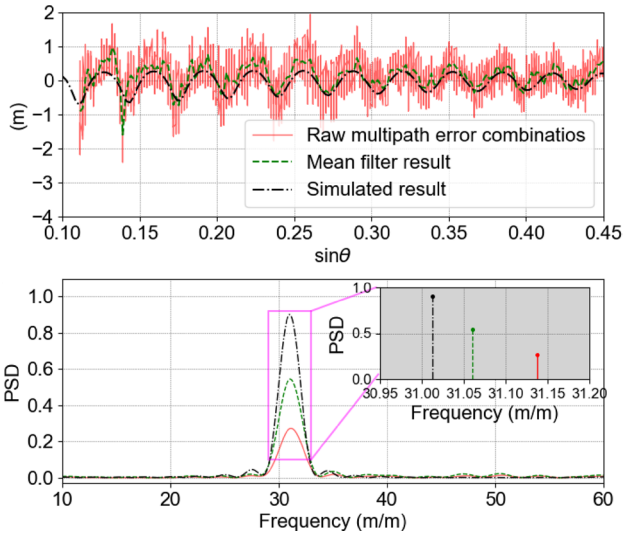

Fig. 5 Time series of raw combination of multipath error (red), mean filter result (green), and the simulated result (black), and the spectrogram for those series

$$\widetilde{M}(t) = \widetilde{\mathrm{CMC}}(t) - \widetilde{2I}(t) \tag{9}$$

Note that, the term of integer ambiguity which is constant could also be removed by (9) after the cycle slip has been detected and repaired.

Figure 4 shows an example of the time series of the raw combinations calculated by (3) and the estimated ionospheric delay calculated by (8) with respect to time t. The output rate of GNSS observations is 1 Hz, and the length of the moving window k is 310 epochs. The estimated ionospheric delay fluctuations show an increasing trend as the elevation angle decreases. This is largely because, as the elevation angle decreases, the length of propagation path through the ionosphere increases, and hence, the TEC (total electron content) increases. Except for the increasing trend, the estimated ionospheric delay also exhibits fluctuations with a period of about 7.5 min; the periodic fluctuation should mainly be induced by the residual multipath error.

After the estimated ionospheric delay is removed from the raw combinations shown in Fig. 4 by (9), the corrected combined multipath errors are produced, as shown in Fig. 5 which also shows the simulated one with the antenna height of 2.98 m. Notice that, since the series of combined multipath errors is a period function of sine of elevation angle, the independent variable in Fig. 5 is sine of satellite elevation angle at the real time t. Since the independent time variable $\sin(\theta(t))$ is actually unitless, the frequency here does not have units of Hz; instead, it has the unit of meter per meter (m/m) and the fitting coefficient a has a unit of m as mentioned in Tables 1 and 2. It is worth mentioning that the frequency of combined multipath error series shown in the top panel of Fig. 5 (green dash line) can be roughly calculated as follows. The series covers a "time period" of about 0.35 (unitless); with about 11 periods within 0.35, the maximum of the PSD (power spectrum density) is located at about 11/0.35 which correspond to about 31 (m/m). It can be observed that the estimated and simulated results have a good match in terms of oscillating trend and the peak frequency. In addition, the data processing results indicate that the ionospheric delay could be well recovered by (8) when the moving window length k is within 200-350 epochs for the GNSS observations with 1 Hz output rate.

Note that, the raw multipath error combinations with elevation angle difference smaller than 0.1° could be treated as one combination with a given elevation angle. Then, the mean filtering method could be used to improve the signal-to-noise ratio of raw multipath error combinations. It can be seen from Fig. 5 that the mean filtering generates a higher peak spectral density and the spectral peak frequency is closer to the simulated one. This is in accordance with the theoretical analysis related to Fig. 2. In addition, the violent fluctuation of the ionosphere, which is often caused by solar flares, earthquake, or hurricane, might lead to the failure of ionospheric removal.

Experimental results

Two field GNSS data sets with a sampling period of 1 s are used to test the proposed snow depth estimation method; the data sets are collected in Harbin, China, and Colorado, USA, respectively. The multi-satellites snow depth estimations with a given GNSS constellation and the signal band for both two experiments are averaged once per day to compare with the in situ data. Note that, two average results (normal average or PM-NA, weighted average or PM-WA) for the

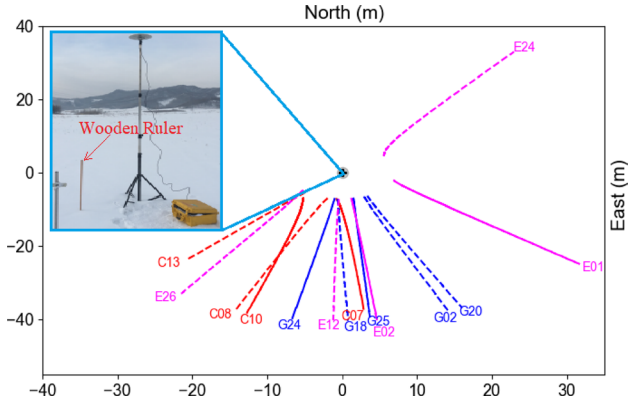

Fig. 6 Local environment around the GNSS receiver. The dash and solid lines represent the specular reflection footprint of descending satellite and ascending satellite, respectively

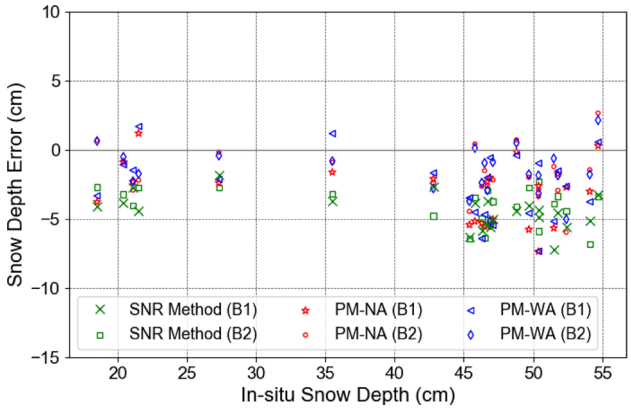

Fig. 8 Snow depth estimation errors for BDS B1 and B2 band signals

Fig. 7 GNSS-R-based daily average snow depth observations and in situ snow depth observations

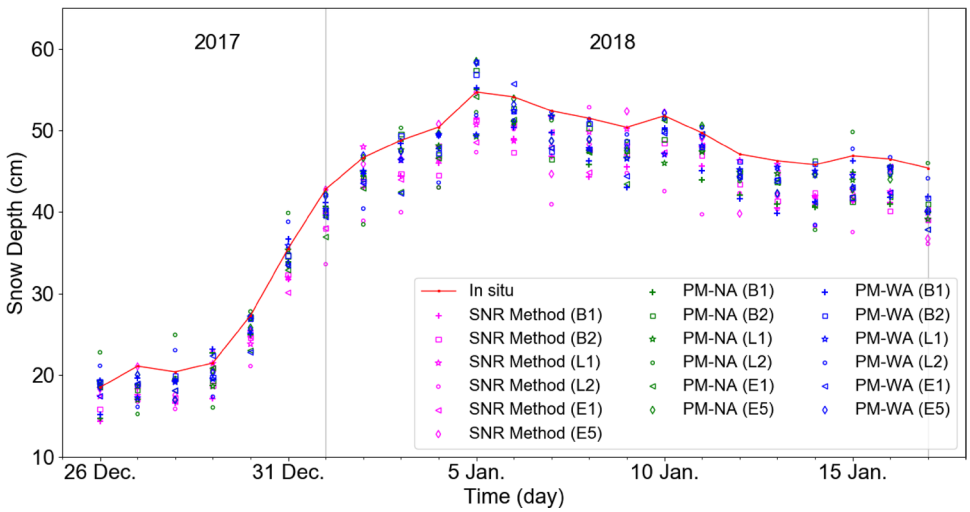

proposed method are presented in this section; the results of PM-NA are calculated by averaging snow depth estimations of multiple satellites each day for a given GNSS frequency signal, while the PM-WA ones are calculated as the weighted average of those snow depth estimations through (7).

Experiment conducted in Harbin, China

The experimental campaign was conducted in northeast China, from December 26, 2017 to January 17, 2018. The Trimble NetR9 GNSS receiver equipped with GNSS antenna TRM55971.00 was used for data collection in the experimental campaign. As shown in Fig. 6, the GNSS antenna was fixed on a pole which was installed in a flat and open area. The height of the GNSS antenna is 3.43 m when the surface is snow-free. GNSS data of 14 satellites with an elevation angle range of 5°–30° are used to test the performance of the proposed method. Note that, the footprints of specular reflection for those satellites when the antenna height is 3.43 m are also shown in Fig. 6. A wooden ruler of one-meter length was used to measure the ground truth snow depth three times a day. Since the difference between the three individual ruler-based daily snow depth measurements and their average measurement is smaller than 1.5 cm for most of the days, the latter is treated as the daily in situ snow depth to compare with GNSS-based snow depth estimations. Figure 7 shows the in situ snow depth observations and the daily average snow depth observations obtained by the SNR method and the proposed method for BDS, GPS, and Galileo.

Figure 8 shows the scatterplot of BDS-based snow depth estimation errors obtained by the SNR method and the proposed method with two band signals. The Mean, STD, and RMS of BDS-based snow depth estimation errors are shown in Table 3. Note that BDS stands for BeiDou Navigation Satellite System. It can be observed that for both methods, there exists an obvious negative mean error. The reason behind this underestimation is the interference of reflected GNSS

Table 3 Mean, STD, and RMS of BDS-based snow depth estimation error

Method	Band	Mean (cm)	STD (cm)	RMS (cm)
SNR	B1	−4.45	1.23	4.61
	B2	−4.06	1.34	4.28
PM-NA	B1	−3.09	2.22	3.81
	B2	−1.90	2.01	2.77
PM-WA	B1	−2.60	2.40	3.54
	B2	−1.61	1.75	2.38

signals coming from underneath of snow surface (Yu et al. 2018).

The proposed method has a smaller mean error than that of the SNR method, probably because the GNSS signals reflected from underneath the snow surface have a smaller effect on the pseudorange and carrier phase multipath errors (Liu and Amin 2007). The STD of the SNR method with the two BDS band signals is significantly smaller than the proposed method, even though the estimation error RMS of the SNR method is larger. Certainly, it is useful to make a correction for the systematic error resulting in underestimation of snow depth to improve the accuracy of snow depth estimation. However, the systematic error is related to the characterization of snow (e.g., density, depth, and temperature) and GNSS signals (e.g., wavelength or frequency, and signal strength), and the relationship is unclear. It is thus desirable to establish the relationship between the systematic error and the different factors in the future.

The weighted average of snow depth estimations of the proposed method performs better than the normal average for the two band signals, although the improvement is not very significant. In addition, the snow depth estimations with B2 band signal are considerably better than that with B1 band signal for the proposed method. The main reason would be that the bandwidth of the B2 signal is 20.46 MHz, much larger than the 4.092 MHz of B1 signal. A higher signal bandwidth will result in a larger SNR (about 39 dB for the BDS B1 band signal in elevation angle of 5°–30°, and about 40 dB for the BDS B2 band signal), and thus, a combined multipath error series with a larger SNR produces more accurate snow depth estimations.

Figure 9 shows the scatterplot of GPS-based snow depth estimation errors with L1 and L2 band signals. It can be observed that the snow depth estimation errors of the GPS L2 band signal are significantly larger than that of the L1 band signal for both methods. This can also be seen from Table 4, which shows the Mean, STD, and RMS of GPS-based snow depth estimation error. The main reason for this is that the strength of legacy GPS signal L2P(Y) is considerably lower than that of the L1 signal strength, as shown in Fig. 10. Therefore, the accuracy of the SNR method and the

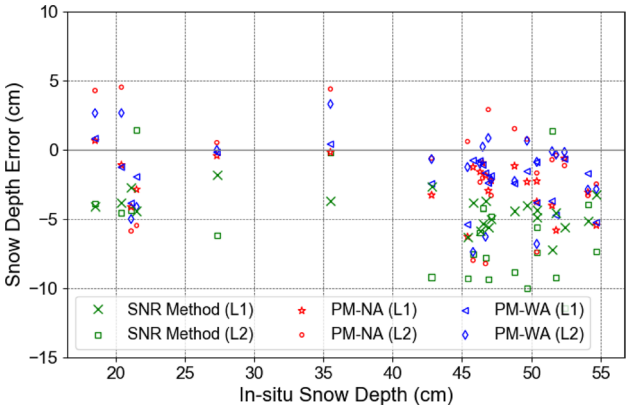

Fig. 9 Snow depth estimation errors for GPS L1 and L2 band signals

Table 4 Mean, STD, and RMS of GPS-based snow depth estimation error

Method	Band	Mean (cm)	STD (cm)	RMS (cm)
SNR	L1	−2.54	1.88	3.16
	L2	−6.01	3.48	6.95
PM-NA	L1	−2.48	1.83	3.08
	L2	−1.45	3.78	4.05
PM-WA	L1	−2.06	1.71	2.68
	L2	−1.47	2.93	3.28

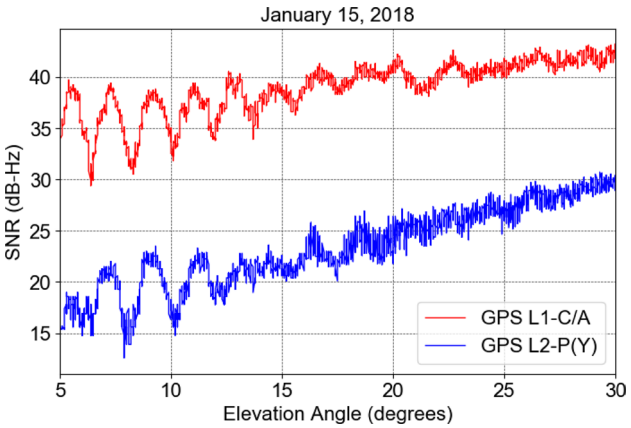

Fig. 10 SNR observations for an ascending GPS satellite with satellite number 25

proposed method with the L1 band signal is better than that with L2P(Y) signal. Because the strength of modernized GPS signal L2C is much higher than that of L2P(Y) signal (Tabibi et al. 2017), the performance of the former would be better for both methods.

Figure 11 shows the scatterplot of Galileo-based snow depth estimation errors with observed data of Galileo E1 and E5 band signals. The Mean, STD, and RMS of Galileo-based

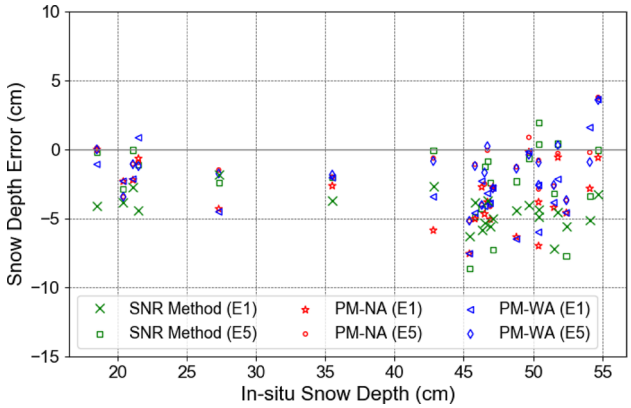

Fig. 11 Snow depth estimation errors for Galileo E1 and E5 band signals

Table 5 Mean, STD, and RMS of Galileo-based snow depth estimation error

Method	Band	Mean (cm)	STD (cm)	RMS (cm)
SNR	E1	−3.36	1.77	3.80
	E5	−2.29	2.76	3.59
PM-NA	E1	−3.46	2.19	4.09
	E5	−1.58	1.96	2.52
PM-WA	E1	−2.78	2.58	3.79
	E5	−1.61	1.85	2.45

snow depth estimation error are shown in Table 5. Using the E5 signal produces better performance than using the E1 signal for the proposed method. The performance gain comes from the smaller pseudorange measurement error with the E5 signal. As studied by Braasch and Dierendonck (1999), the accuracy of pseudorange measurement is inversely proportional to the pseudorandom noise code period, which is 244.4 ns for C1X of the Galileo E1 signal and 97.8 ns for C8X of the Galileo E5 signal. The smaller code period produces smaller measurement noise and more accurate snow depth estimations.

Figure 12 shows a comparison of error Mean, STD, and RMS between the proposed method, the dual-frequency pseudorange and carrier phase combination method (Yu et al. 2018), and the triple-frequency carrier phases combination method (Yu et al. 2015). DC and TC stand for dual-frequency method and triple-frequency method, respectively. For example, DC (L1L2) is the dual-frequency combination of GPS L1 pseudorange, L1 carrier phase, and L2 carrier phase, while DC (L2L1) is the dual-frequency combination of GPS L2 pseudorange, L2 carrier phase, and L1 carrier phase; TC (L1L2L5) is the triple-frequency combination of GPS L1 carrier phase, L2 carrier phase, and L5 carrier phase. The daily averages are used to calculate the error Mean, STD, and RMS for the two methods (DC and TC). Note that, the Trimble R9 receiver used in our experiment cannot process BDS B3 signal, so the triple-frequency method is unavailable for BDS; the GPS results

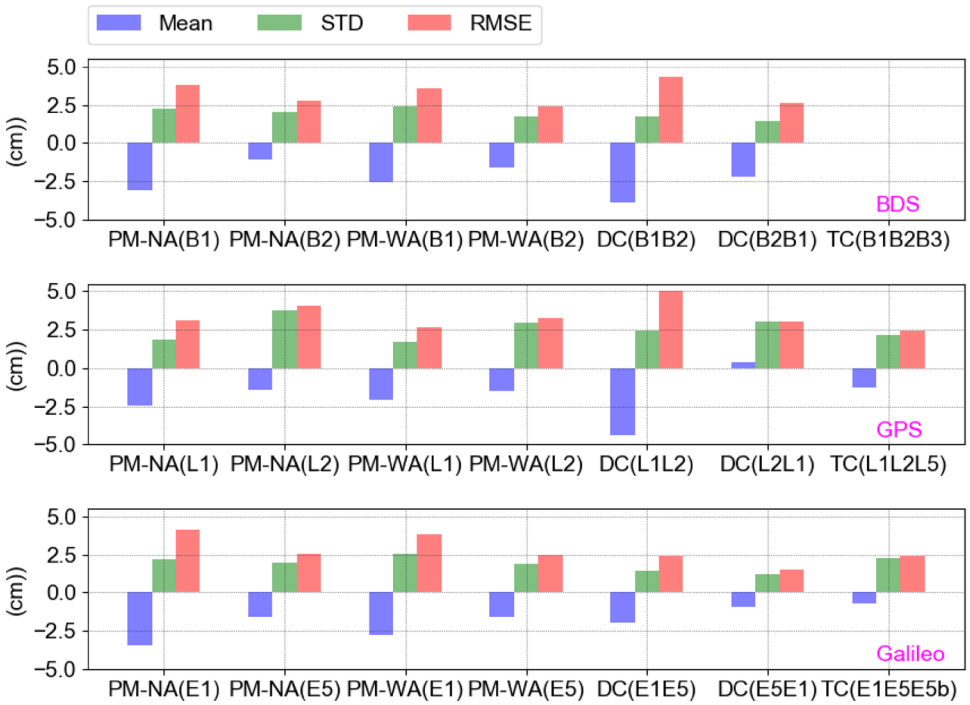

Fig. 12 Comparison of error Mean, STD, and RMS for the proposed method, dual-frequency combination method, and triple-frequency combination method

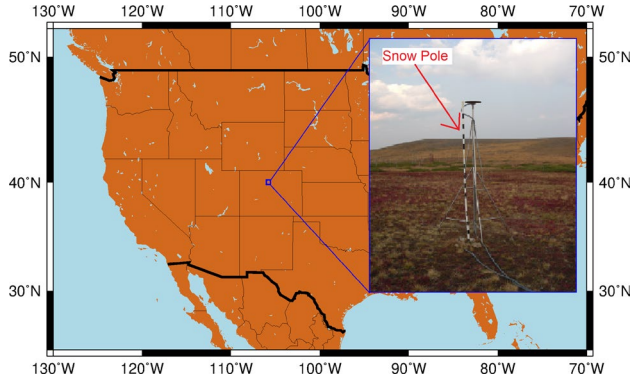

Fig. 13 Location (latitude and longitude) of GPS station as well as ground conditions in the vicinity of GPS station

of triple-frequency method are obtained by data associated with two satellites (#24 and #25).

It can be seen that there is no significant difference in the snow depth estimation performance between the proposed method and dual-frequency method in general. The reason for this should be that the ionospheric fluctuation is relatively stable and slow during the experiment, and the ionospheric delays are well estimated and removed from the raw combination by (8) and (9). The performance of the triple-frequency method is better than the proposed method and the dual-frequency method with GPS data, while the dual-frequency method with Galileo E1 and E5 data yields the best result. This could be because the multipath error signal of pseudorange is much larger than that of carrier phase and the measurement noise of Galileo E5 signal is relatively small, producing higher signal-to-noise series of combined multipath error and more accurate snow depth estimations. Note that, as mentioned before, the violent fluctuation of the ionosphere might lead to the failure of ionospheric removal and hence produce large snow depth estimation errors for the proposed single-frequency method. Thus, the dual- and triple-frequency methods which are free of ionospheric errors are preferable for snow depth estimations in the presence of multi-frequency GNSS observations.

NWOT, USA

This experimental data set is provided by the Plate Boundary Observatory operated by UNAVCO for EarthScope (http://xenon.colorado.edu/portal/index.php). The GPS station called NWOT is installed on the top of a saddle-like mountain of Niwot Ridge in CO, USA, as shown in Fig. 13. The station is equipped with a Trimble NetR8 GPS receiver and Trimble 41,249.00 antenna, and only GPS observations are recorded. There is a complicate reflection environment around station NWOT. The reflection surface is rough and the topographical slopes range from 2° to 7°, with an average

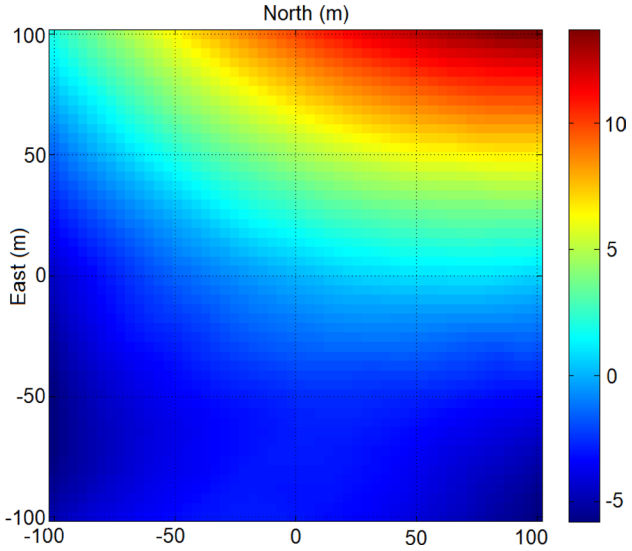

Fig. 14 Digital elevation model around the GPS station NWOT

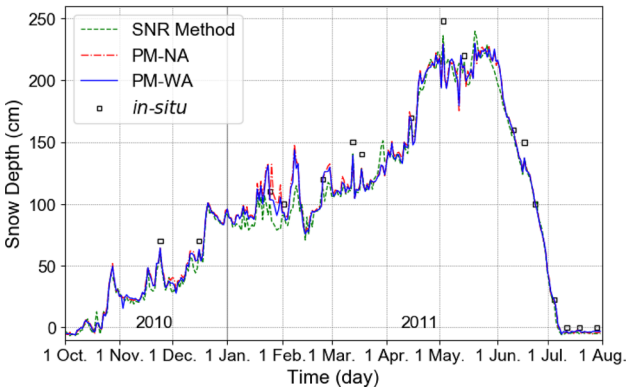

Fig. 15 Daily snow depth estimations in NWOT

of about 5° within 50 m radius around the GPS station, as shown in Fig. 14. Data of 32 GPS satellites with an azimuth of footprints of specular reflection ranging from 90° to 270° are used to evaluate the performance of the proposed method, as the ground surface on the south of the station is relatively flat in the absence of a snowpack. A snow pole of 3 meters length was used to measure the in situ snow depth, but there are only a rather limited number of in situ snow depth measurements during a year.

Because the pseudorange and carrier phase combination of GPS L1 signal achieves a better performance than that of L2 signal, as shown in Table 4, only the snow depth estimations based on the L1 signal are presented. Figure 15 shows the daily snow depth estimates obtained by the SNR method and the proposed method during the winter season between 2010 and 2011. In addition, in situ data are also displayed. It can be observed that the variation of snow depth is well captured by the SNR method and the proposed method. In early

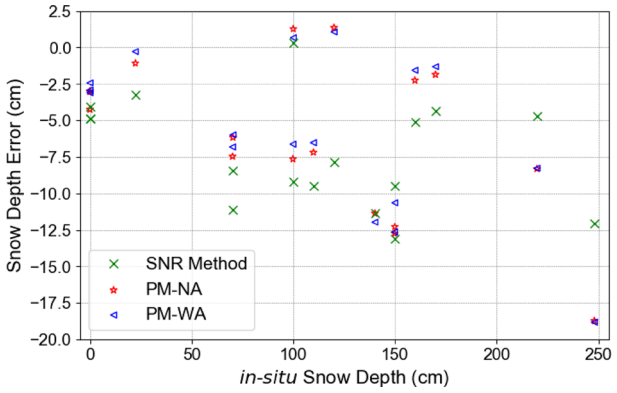

Fig. 16 Snow depth estimation errors in NWOT

Table 6 Mean, STD, and RMS of GPS-based snow depth estimation error in NWOT

Method	Mean (cm)	STD (cm)	RMS (cm)
PM-NA	−6.16	5.43	8.21
PM-WA	−5.77	5.42	7.92

October 2010 and July 2011, the ground around the GPS station is snow-free. However, both the SNR method and the proposed method generate negative snow depth estimations. Except for the reason of topographical slopes around the GPS station, some components of the GPS signal might penetrate the soil and are reflected from the inner soil layer with longer propagation paths, resulting in overestimated antenna height.

Figure 16 shows the snow depth estimation errors versus the in situ snow depth observations for the SNR method, the averaged proposed method, and the weighted proposed method. Obviously, the estimation error of station NWOT is much larger than that of data collected in northeastern China for both methods, as shown in Fig. 9. This can also be observed from Table 6, which shows the Mean, STD, and RMS of the snow depth estimation error in NWOT. The main reason for this should be the in situ snow depth is based on point observable, while the GPS-based snow depth estimations represent the averaged snow depth of an area which has a slope snow surface.

As the ground slopes would produce a significant error on the snow depth estimation, it is necessary to make topographic corrections for the GNSS-R-based snow depth estimations. The topographic correction for each satellite could be estimated as the difference between the geometrical antenna height (from its top point to its bottom point) and the estimated antenna height for the bare snow-free ground (Larson et al. 2008),

$$\Delta H_i^{\text{corr}} = H - \overline{H}_i^{\text{ground}} \tag{10}$$

where $\overline{H}_i^{\text{ground}}$ is the antenna height estimated by the proposed method when the ground is bare and snow-free. Then, the topographic-corrected antenna height estimate with the snow-covered ground is given by:

$$h_i^{\text{corr}} = h_i + \Delta H_i^{\text{corr}} \tag{11}$$

where h_i is the original GNSS-based antenna height estimate.

To increase the accuracy of $\overline{H}_i^{\text{ground}}$, the antenna height above the bare snow-free ground is estimated over 20 days of two different snow-free periods. The first period is from October 1, 2010 to October 10, 2010 prior to the snowfall season, while the second one is from July 10, 2011 to July 20, 2011 posterior to the snowfall season. Twenty individual topographic corrections are averaged to generate a topographic correction for each satellite. Because the ground reflection tracks are repeatable for each satellite when the ground is snow-free, the change of antenna height above the bare ground is marginal over the 20 days for most of the satellites, as shown in Fig. 17 where bare ground heights and topographic corrections for ten satellites are displayed. Note that, a longer period for calculating the topographic correction is not recommended, as the height of vegetation around the station would produce a significant effect on the bare ground height, especially in summer.

Figure 18 shows the scatterplot of topographic-corrected snow depth estimations versus the in situ snow depth observations for the averaged and weighted averaged schemes of the proposed method. To some extent, the negative topographic bias has been removed from the GPS-based snow depth estimations, especially when the snow depth is small. This can also be observed from Table 7, which shows the error Mean, STD, and RMS of the topographic-corrected snow depth estimations in NWOT. The ground reflection tracks are unrepeatable when the snow depth changes and the topographic correction for the bare ground track cannot correct the topographic bias exactly in the snowfall season. In addition, the uneven distribution of snow depth would also cause estimation errors, especially for the sloped surface. Nevertheless, the topographic correction significantly improves the snow depth estimation as evidenced by Table 7.

Concluding remarks

A new snow depth estimation method which uses a combination of pseudorange and carrier phase observations of GNSS single-frequency signal has been proposed. The proposed method is more applicable, as the single-frequency pseudorange and carrier phase observations can always be obtained from a typical GNSS receiver. Theoretical linear models describing the relationship between antenna height

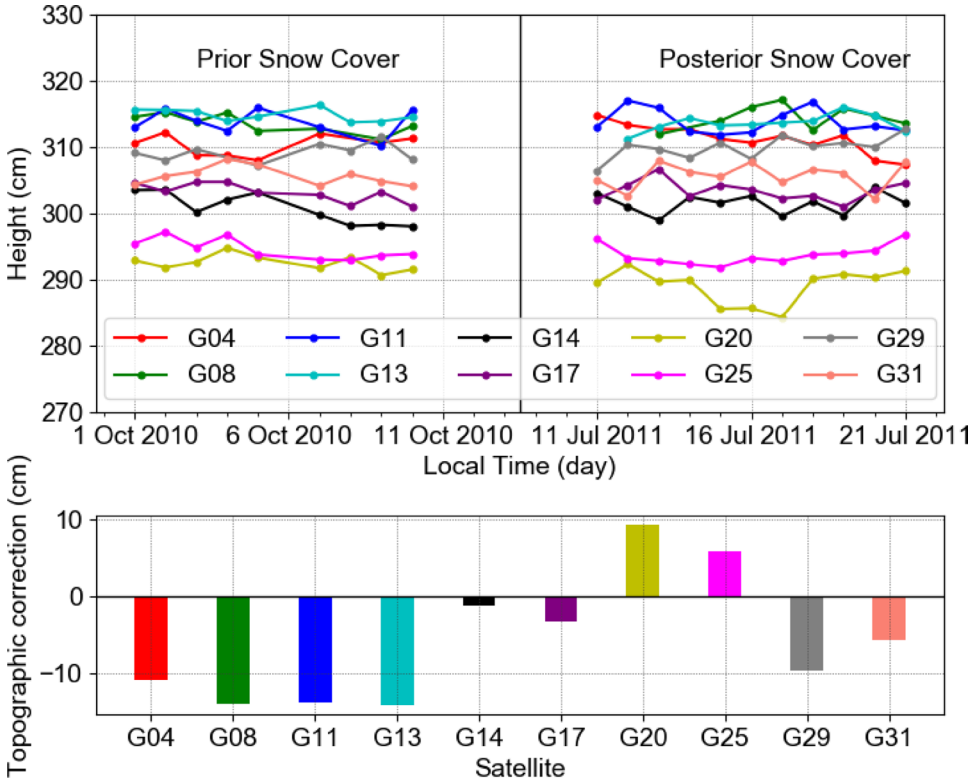

Fig. 17 Example of estimated antenna heights above bare ground obtained by the proposed method (top), and topographic corrections (bottom)

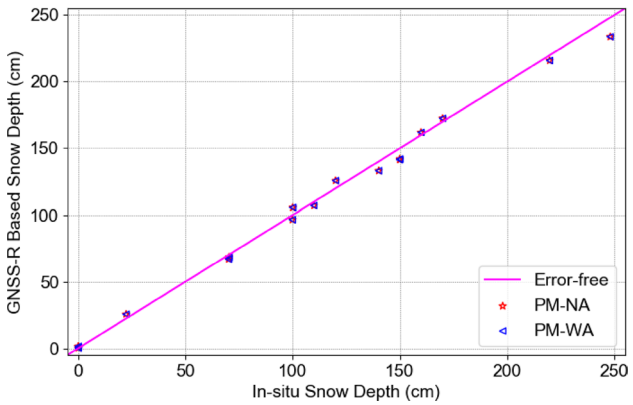

Fig. 18 Scatterplot of topographic-corrected snow depth estimations versus the in situ snow depth observations

Table 7 Mean, STD, and RMS of topographic-corrected snow depth estimation error in NWOT

Method	Mean (cm)	STD (cm)	RMS (cm)
PM-NA	−1.82	5.43	5.72
PM-WA	−1.45	5.17	5.37

and peak frequency of the combined multipath error series have been developed. Theoretical analysis and simulation show that the antenna gain pattern and snow permittivity have a marginal impact on the peak frequencies of the combined multipath error series. Those models are GNSS signal frequency-related and are independent of satellite selection and measurement location, if the reflection surface is basically flat. In addition, a weighting method has been proposed for combining multiple snow depth estimates generated from observations related to multiple individual GNSS satellites.

We test the proposed method by single-frequency observations recorded by multi-frequency geodetic-grade receivers. Since there is a difference in measurement noise level and in the multipath error signal between a geodetic-grade receiver and a low-cost single-frequency receiver, e.g., u-blox m8t, the proposed method also needs to be verified with the data collected by the latter in the future research. In order to improve the accuracy of GNSS-based snow depth estimation, future research will also focus on weighting the snow depth observations of different band signals, different GNSS constellations, and different GNSS-based snow depth estimation methods.

Acknowledgements This work was supported by the National Natural Science Foundation of China under Grants 41574031 and 41730109, Advanced Research Projects of the 13th 5-year Plan of Civil Aerospace Technology, and Key Laboratory of Geospace Environment and Geodesy, Ministry of Education, Wuhan University under Grant Number

17-02-07. The authors would like to thank the anonymous reviewers for their valuable comments and suggestions.

References

Axelrad P, Larson KM, Jones B (2005) Use of the correct satellite repeat period to characterize and reduce site-specific multipath errors. In: Proceedings of the ION GNSS 2005, The Institute of Navigation, Long Beach, CA, Sept 2005, pp 2638–2648

Barry RG (1996) The parameterization of surface albedo for sea ice and its snow cover. Prog Phys Geogr 20(1):63–79

Blanco-Delgado N, Haag MUD (2011) Multipath analysis using code-minus-carrier for dynamic testing of GNSS receivers. In: 2011 international conference on localization and GNSS (ICL-GNSS), Tampere, 2011, pp 25–30

Braasch MS, Dierendonck AJ (1999) GPS receiver architectures and measurements. Proc IEEE 87(1):48–64

Estilow TW, Young AH, Robinson DA (2015) A long-term northern hemisphere snow cover extent data record for climate studies and monitoring. Earth System Science Data 7(1):137–142

Garvelmann J, Pohl S, Weiler M (2013) From observation to the quantification of snow processes with a time-lapse camera network. Hydrol. Earth System Science Data 17:1415–1429

Harpold AA et al (2014) Lidar-derived snowpack data sets from mixed conifer forests across the western united states. Water Resour Res 50(3):2749–2755

Henkel P, Koch F, Appel F, Bach H, Prasch M, Schmid L, Schweizer J, Mauser W (2018) Snow water equivalent of dry snow derived from GNSS carrier phases. IEEE Trans Geosci Remote Sens 56(6):3561–3572

Jin S, Najibi N (2014) Sensing snow height and surface temperature variations in Greenland from GPS reflected signals. Adv Space Res 53(11):1623–1633

Larson KM, Small EE, Gutmann E, Billich A, Braun JJ, Zavorotny VU (2008) Use of GPS receivers as a soil moisture network for water cycle studies. Geophys Res Lett 35(24):851–854

Liu L, Amin MG (2007) Comparison of average performance of GPS discriminators in multipath. In: 2007 IEEE international conference on acoustics, speech and signal processing—ICASSP'07, Honolulu, HI, vol 2007(3), pp 1285–1288 https://doi.org/10.1109/icassp.2007.367079

Lomb NR (1976) Least-squares frequency analysis of unequally spaced data. Astrophys Space Sci 39(2):447–462

Nievinski FG, Larson KM (2014a) Inverse modeling of GPS multipath for snow depth estimation—part II: application and validation. IEEE Trans Geosci Remote Sens 52(10):6564–6573

Nievinski FG, Larson KM (2014b) Forward modeling of GPS multipath for near-surface reflectometry and positioning applications. GPS Solut 18(2):309–322

Ozeki M, Heki K (2012) GPS snow depth meter with geometry-free linear combinations of carrier phases. J Geodesy 86(3):209–219

Pugliano G, Robustelli U, Rossi F, Santamaria R (2016) A new method for specular and diffuse pseudorange multipath error extraction using wavelet analysis. GPS Solut 20(3):499–508

Scargle JD (2003) Studies in astronomical time series analysis II—statistical aspects of spectral analysis of unevenly spaced data. Astrophys J 263(2):835–853

Serreze MC, Clark MP, Armstrong RL, McGinnis DA, Pulwarty RS (1999) Characteristics of the western United States snowpack from snowpack telemetry (SNOTEL) data. Water Resour Res 35(7):2145–2160

Small EE, Larson KM, Braun JJ (2010) Sensing vegetation growth with reflected GPS signals. Geophys Res Lett 37(12):245–269

Sturm M (2009) Field techniques for snow observations on sea ice. In: Eicken H, Bluhm B, Collins RE, Gradinger R, Haas C, Ingham M, Mahoney AR, Nicolaus M, Perovich D (eds) Field techniques for sea ice research. University of Alaska Press, Fairbanks, pp 25–47

Tabibi S, Nievinski FG, Dam TV (2017) Statistical comparison and combination of GPS, GLONASS, and multi-GNSS multipath reflectometry applied to snow depth retrieval. IEEE Trans Geosci Remote Sens 55(7):3773–3785

Tiuri M, Sihvola A, Nyfors E, Hallikaiken M (1984) The complex dielectric constant of snow at microwave frequencies. IEEE J Ocean Eng 9(5):377–382

Wellenhof BH, Lichtenegger H, Wasle E (2008) GNSS-global navigation satellite system: GPS, GLONASS, Galileo and more. Springer-Verlag, New York

Yu K, Rizos C, Dempster A (2014) GNSS-based model-free sea surface height estimation in unknown sea state scenarios. IEEE J Sel Top Appl Earth Observ Remote Sens 7(5):1424–1435

Yu K, Ban W, Zhang X, Yu X (2015) Snow depth estimation based on multipath phase combination of GPS triple-frequency signals. IEEE Trans Geosci Remote Sens 53(9):5100–5109

Yu K, Li Y, Chang X (2018) Snow depth estimation based on combination of pseudorange and carrier phase of GNSS dual-frequency signals. IEEE Trans Geosci Remote Sens 57(3):1817–1828

Yunwei Li received the B.S. degree in the College of Geomatics, Shandong University of Science and Technology, Qingdao, China, in 2011; and M.S. degree in geodesy from the School of Geodesy and Geomatics, Wuhan University, Wuhan, China, in 2019. He is currently working toward the Ph.D. degree in the School of Geodesy and Geomatics, Wuhan University.

Xin Chang received the B.S. degree and M.S. degree in geodesy from the School of Geodesy and Geomatics, Wuhan University, Wuhan, China, in 2012 and 2015, respectively. He is currently working toward the Ph.D. degree in the School of Geodesy and Geomatics, Wuhan University.

Kegen Yu received the Ph.D. degree in electrical engineering from the University of Sydney, Sydney, NSW, Australia, in 2003. He is currently a Professor with the School of Environmental Science and Spatial Informatics, China University of Mining and Technology, Xuzhou, China.

Shuyao Wang received the B.S. degree in geodesy from the School of Geodesy and Geomatics, Wuhan University, Wuhan, China, in 2017. She is currently working toward the M.S. degree in the School of Geodesy and Geomatics, Wuhan University.

Jiancheng Li received the Ph.D. degree in Department of Geodesy, Wuhan Technical University of Surveying and Mapping, Wuhan, China, in 1993. He is currently a Professor with the School of Geodesy and Geomatics, Wuhan University, Wuhan, China.